Lattice instabilities and phonon thermal transport in TlBr

Tribhuwan Pandey, Lucas Lindsay, Brian C. Sales, and David S. Parker

Materials Science and Technology Division, Oak Ridge National Laboratory, Oak Ridge, Tennessee 37831, USA

Materials with simple crystal structure usually exhibit substantial lattice thermal conductivity (κ_{latt}) due to a scarcity of strong phonon-phonon scattering channels. Yet here we find simple CsCl-structure TlBr to have an extremely *low* room temperature $\kappa_{latt} \sim 0.5$ W/m-K, while at low temperature we find a *high* κ_{latt} of 155 W/m-K. This extreme range of conductivity behavior results from lattice-instability-related anharmonicity, effective only at temperatures above $\sim$30 K. Manipulating these instabilities (e.g., pressure, strain) may yield a pathway to ultralow thermal conductivity via intrinsic phonon resistance in similar materials.

I. INTRODUCTION

Crystalline solids with ultralow lattice thermal conductivity (κ_{latt}) are essential for the development of energy efficient thermal devices (e.g., thermoelectrics). Extrinsic strategies such as alloying [1,2] and nanostructuring [3–5] are effective in reducing κ_{latt}, but often yield an undesirable reduction of electrical mobility as lattice defects also scatter electrons. Solids with intrinsically low κ_{latt} strategically offer optimal thermal properties without degrading electronic behaviors. Ultralow κ_{latt} is often realized in materials with a complex unit cell with heavy atoms, low atomic density, and small Debye temperature. These factors determine the so-called "lower" limit of κ_{latt} at high temperatures (κ_{min}) as proposed by Slack (Slack model) [6] and Cahill, Watson, and Pohl (CWP model) [7]. The Slack κ_{min} model [6] approximates contributions from both acoustic and optic phonons, while the CWP model [7] describes κ_{min} in terms of acoustic phonon characteristics only and describes hopping of vibrational energy. In recent years, several modifications to the CWP model have been posited to explain the limiting κ_{latt} behaviors in crystalline and disordered materials, including one recently proposed by Agne *et al.* [8], in which the lower κ_{latt} limit is described by diffuson-mediated transport. On a similar note, Mukhopadhyay *et al.* [9] proposed that for ultralow κ_{latt} materials heat is transported by two vibrational channels, a "hopping" channel (described by the CWP model or that proposed by Einstein [10]) and the usual phonon conduction channel. The combination of these two transport channels (hopping and phonon) attained better agreement with the measured thermal conductivities in various ultralow κ_{latt} materials for which the phonon conduction channel alone failed. Recently, methods [11,12] have also been proposed to calculate thermal transport from both particlelike phonons (diagonal terms) and wavelike tunneling and loss of coherence between different vibrational eigenstates (off diagonal terms) of the heat current operator [13]. These methods show that including contributions from off-diagonal elements improves the agreement with experimental measurements in low thermal conductivity materials.

Partly motivated by these studies, in this Rapid Communication we focus on lattice dynamics and thermal transport (experiment and theory) in diatomic TlBr, commonly used in

γ-ray detectors [14–18]. We show that despite its very simple crystal structure (CsCl structure) TlBr exhibits an ultralow κ_{latt} of 0.5 W/m-K at room temperature (RT). Despite this, it has a relatively large measured peak κ_{latt} (155 W/m-K) at low temperature. From first principles calculations, phonons in TlBr exhibit two main lattice instabilities: a soft acoustic mode instability at the *M* point and proximity to a ferroelectric instability [transverse optical (TO) vibration at the Γ point]. These instabilities, together with the bath of other low frequency TO phonons, induce strong anharmonic scattering of heat carrying acoustic and optic phonons. This coupled with low phonon group velocities results in ultralow κ_{latt}. As in Tl_3VSe_4 [9], a two-channel model gives improved agreement of calculations and measurements in TlBr.

II. METHODOLOGY

The key ingredients for computing lattice thermal conductivity are harmonic and anharmonic interatomic force constants (IFCs), which govern phonon dynamics and interactions. These IFCs are estimated from supercell displacement techniques as implemented in PHONOPY [19,20] and PHONO3PY [19,21] and based on first principles density functional theory (DFT) calculations within the generalized gradient approximation and using the Perdew-Burke-Ernzerhof (PBE)sol [22] exchange-correlation functional as implemented in VASP [23–25]. For the harmonic IFCs, atoms were displaced by 0.02 Å in $6 \times 6 \times 6$ supercells (432 atoms) using a $2 \times 2 \times 2$ *k* mesh and energy cutoff of 600 eV. The long-range anisotropic dipole-dipole interactions were treated according to a method proposed by Gonze *et al.* [26,27]. For the third order IFCs, atoms were displaced by 0.03 Å in $5 \times 5 \times 5$ supercells (250 atoms) using Γ-point-only sampling and energy cutoff of 600 eV. For these calculations, all possible triplet interactions within the supercells were included. The harmonic and anharmonic IFCs were used to calculate κ_{latt} by full solution of the Boltzmann transport equation as implemented in the PHONO3PY code [19,21] and including mass variance scattering from the natural isotope composition. The Brillouin zone integration was performed by the tetrahedron method using a $31 \times 31 \times 31$ mesh.
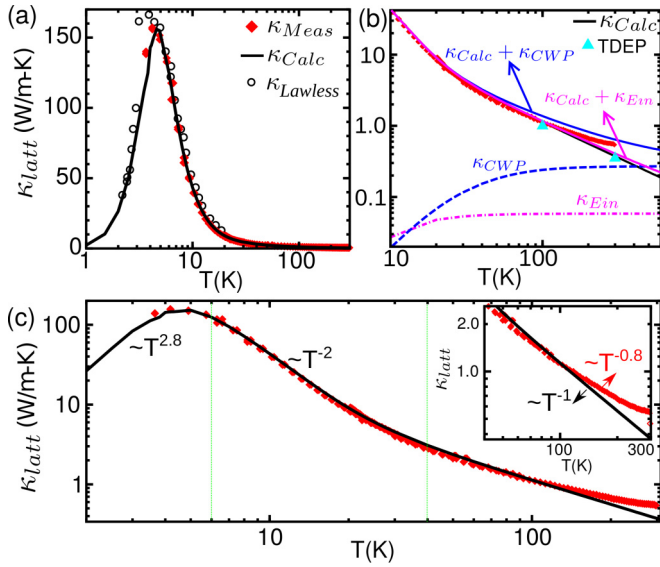
FIG. 1. (a) Measured (κ_{Meas}) and calculated (κ_{Calc}) lattice thermal conductivity as a function of temperature. Previous low temperature (2–20 K) thermal conductivity measurements of Lawless [29] (κ_{Lawless}) are also shown by black open circles. (b) Vibrational thermal conductivity determined by Einstein oscillators (κ_{Ein}) and the Cahill-Watson-Pohl (κ_{CWP}) model as a function of temperature. Also shown are these hopping transport models combined with κ_{Calc}. Cyan triangles in (b) correspond to lattice thermal conductivity calculated with force constants from the temperature dependent effective potential (TDEP) approach. (c) Temperature dependence of κ_{Meas} and κ_{Calc} in three temperature regions. For $T > 40$ K, κ_{Meas} deviates from T^{-1} behavior and decays as $T^{-0.8}$.

Comparison of κ_{latt} obtained from full solution [κ_{Calc} (full-sol)] and using the relaxation time approximation [κ_{Calc} (RTA)] is shown in Fig. S1 in the Supplemental Material (SM) [28]. As expected for low κ_{latt} materials, differences between full solution and RTA lattice thermal conductivities are negligible. Measurements of heat capacity and thermal conductivity were made on commercial single crystal samples using Quantum Design commercial equipment. Additional details concerning experimental measurements and thermal conductivity calculations are presented in the SM [28].

III. RESULTS AND DISCUSSION

Measured and calculated κ_{latt} are shown in Figs. 1(a)–1(c). The calculated lattice thermal conductivity (κ_{Calc}) includes thermal resistance from phonon-boundary, phonon-isotope, and three-phonon scattering. A boundary scattering length of $L = 165$ μm was determined by fitting the maxima of measured lattice thermal conductivity (κ_{Meas}). The phonon-boundary scattering rates at low (5 K) and room (300 K) temperatures are compared with corresponding phonon-isotope and phonon-phonon scattering rates in Fig. S2 of the SM [28]. As presented in Fig. 1(c) at low temperatures, the boundary scattering is dominant and κ_{latt} has the expected low temperature ($T < 5$ K) behavior, following nearly $\sim T^{2.8}$ dependence mostly dictated by the specific heat. κ_{latt} peaks at 5 K with a value of 155 W/m-K where phonon-isotope scattering [30,31] is also significant, giving $\sim 26\%$ reduction (for this choice

of L) compared with isotopically pure TlBr, mainly from the Tl isotope disorder (29.52% Tl^{203}, 70.48% Tl^{205}). For temperature in the range $6 \leqslant T \leqslant 40$ K, both κ_{Meas} and κ_{Calc} decay as T^{-2}. At higher temperatures ($T > 40$ K), phonon-phonon scattering is dominant and the κ_{Calc} varies approximately as T^{-1}. Similar to the thermal conductivity behavior of Tl_3VSe_4 [9], for $T > 40$ K κ_{Meas} of TlBr begins to vary significantly from κ_{Calc} and decreases with a slower temperature dependence of $\sim T^{-0.8}$ [inset of Fig. 1(c)]. At RT κ_{Calc} is 0.38 W/m-K, while κ_{Meas} is 0.49 W/m-K. Regardless of this discrepancy, these values are surprisingly low for a simple cubic diatomic crystal. In addition, the κ_{peak} to κ_{RT} ratio $[\frac{\kappa_{\text{peak}}}{\kappa_{\text{RT}}}]$ is remarkably large ~ 320, indicating that TlBr exhibits both high (at low temperatures) and ultralow (at temperatures greater than 30 K) thermal conductivity. As shown in Fig. 1(a) our low temperature κ_{Meas} is in good agreement with previous low temperature measurements of Lawless [29] where a maximum κ_{latt} of ~ 166 W/m-K was observed at ~ 4 K.

To better understand the observed κ_{latt} behavior, we measured and calculated the heat capacity (C), which is shown in Fig. 2(a) scaled by T^3. This temperature scaling is used to highlight non-Debye-like behavior at low temperatures. C/T^3 has a broad peak centered at $T = 6.6$ K demonstrating Einstein oscillator behavior with an average Einstein temperature (Θ_{E}) of 30.7 K (0.64 THz), in agreement with the previous measurements of Lawless [29]. From the point of view of the harmonic phonon dispersion, this behavior arises from flat acoustic branches in this frequency region, as can be seen by a peak in the calculated density of states in Fig. 2(b). As postulated recently [9], strong anharmonic scattering confines phonon mean free paths to the order of a lattice spacing (Ioffe-Regel limit [32]) at RT, for which their vibrational energy may propagate by a hopping transport channel described by one of the minimum conductivity models discussed above.

Two models are used to describe this hopping of localized vibrational energy: (1) one proposed by Einstein (κ_{Ein}) and (2) the CWP model (κ_{CWP}) mentioned above. These are shown in Fig. 1(b). Details of these calculations are similar to those given in Ref [9]. The Einstein model requires an oscillator temperature as input, while the CWP model requires the acoustic (transverse TA and longitudinal LA) sound velocities. The Einstein temperature from the heat capacity measurements is used here, while the sound velocities are determined from the calculated phonon dispersion: $TA_1 = 1104$ m/s, $TA_2 = 1140$ m/s, and LA = 2269 m/s. At RT, $\kappa_{\text{Ein}} = 0.058$ W/m-K and $\kappa_{\text{CWP}} = 0.26$ W/m-K. Separately adding these vibrational transport channels with the phonon conductivity ($\kappa_{\text{two-channel}} = \kappa_{\text{latt}} + \kappa_{\text{hopping}}$) we find that the CWP model gives better agreement with the measured data. The two-channel terms bracket the experimental data around RT, similar to the previous comparison for Tl_3VSe_4 [9]. We note that the results discussed above do not include the effects of quartic anharmonicity, which can shift phonon frequencies and provide more scattering channels, even at RT, particularly in strongly anharmonic materials [33–35]. A recent theoretical study asserts that considering phonon renormalization and four-phonon interactions gives better agreement between calculated and measured conductivities of Tl_3VSe_4 [36]. Below we discuss the effects of temperature in shifting phonon frequencies and altering interactions
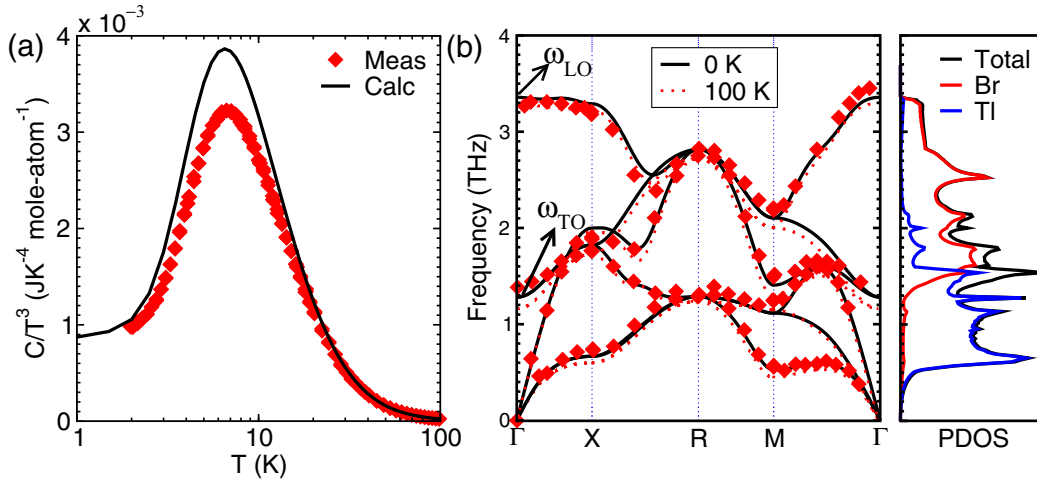
FIG. 2. (a) Comparison of measured (red diamonds) and calculated heat capacity (black solid curve) divided by temperature cubed (C/T^3) as a function of temperature. (b) Calculated phonon dispersions at 0 K (solid black curves) and 100 K (red dotted curves) along with the corresponding projected phonon density of states (PDOS) at 0 K. Red diamonds in (b) represent inelastic neutron scattering data measured at 100 K [39].

within the quasiharmonic approximation and using a more rigorous temperature-dependent effective potential (TDEP) method [30,37,38]. Unfortunately, directly including quartic anharmonicity is beyond the scope of this work.

To build a better understanding of the conductivity behavior in TlBr, we first examine the role of harmonic properties in determining κ_{latt}. Calculated phonon dispersions of TlBr from two separate methods (typical DFT at 0 K calculations and TDEP calculations performed at 100 K (see SM [28]) are compared with measured neutron scattering data [39] at 100 K in Fig. 2(b). 0-K calculations give slightly harder phonons compared with those from the TDEP method at 100 K. In general, the phonon dispersion calculated with the 0 K lattice parameter is in good agreement with the neutron scattering data, whereas the calculated 100-K optic phonon frequencies are slightly lower than the data. This suggests a sensitivity of the phonon structure to lattice expansion, consistent with the strong anharmonicity discussed later. The κ_{latt} calculated with 0 K IFCs and TDEP IFCs [shown by cyan triangles in Fig. 1(b)] are comparable. A comparison of the thermal conductivities from these methods is given in Table I. The discussion presented below is based on the IFCs calculated with the 0-K lattice parameter.

Anticrossing behavior between LA and transverse optic (TO) phonon branches is observed along the $\Gamma - M$ and $\Gamma - X$ directions. A flat TA phonon branch can be seen between Γ and M, which is responsible for the Tl-dominated peak at 0.64 THz in the phonon density of states (PDOS). As shown in the PDOS in Fig. 2(b), the Tl atoms are primarily responsible for the soft acoustic branches and low acoustic group velocities (see above). TlBr has a very large LO-TO splitting ~2.1 THz, greater than half of the overall dispersion. This results from large Born effective charges, which quantify induced lattice polarization with atomic displacements. The calculated Born effective charges are over two times larger (Tl: +2.2, Br: −2.2) than their nominal ionic charges Tl: +1 and Br: −1. These were previously associated with the cross-gap hybridization between the Tl and Br p states resulting

in charge transfer between the nearest-neighbor Tl and Br atoms upon atomic displacement [40]. Materials with such large Born charges are often found to be near a ferroelectric instability, as was observed in PbTe [41–43], GeTe [44], and SnSe [45,46], manifested by soft polar TO phonons near the Γ point [41,43,45,47]. Soft TO modes are also present in the TlBr dispersion near the zone center, indicating that TlBr is close to a ferroelectric instability as previously suggested [40]. However, this is not the only, or even the primary, lattice instability in TlBr. This ferroelectric instability competes with a TA$_1$ instability observed along the $\Gamma - M$ direction, and *both* instabilities are important for generating the low RT κ_{latt}. To investigate this further, we calculated phonon dispersions with lattice parameters expanded by 1%, 1.5%, and 2.0% from the 0 K parameter as shown in Fig. 3(a). While the frequencies of both the TO branch (at the Γ point) and the TA$_1$ branch (at the M point) sharply decrease with increasing lattice parameters, the TA$_1$ frequencies become negative at 2.0% lattice expansion indicating a dynamical instability governed by these. The TO Γ-point frequencies remain positive, though much decreased. We discuss the role of these instabilities in determining the low RT κ_{latt} of TlBr below.
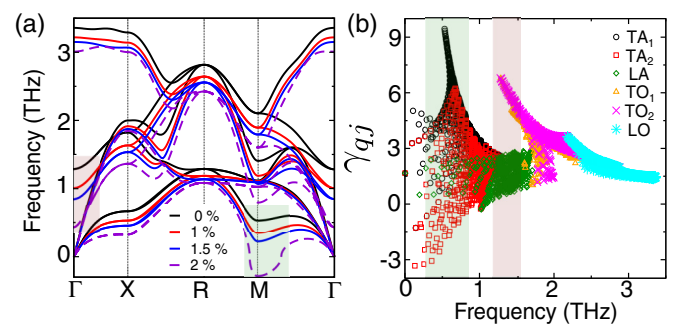

FIG. 3. (a) Phonon dispersions with the 0 K optimized parameter (black solid curves) and 1, 1.5, and 2.0% expanded lattice parameters. (b) Mode decomposed Grüneisen parameters calculated at 0 K.
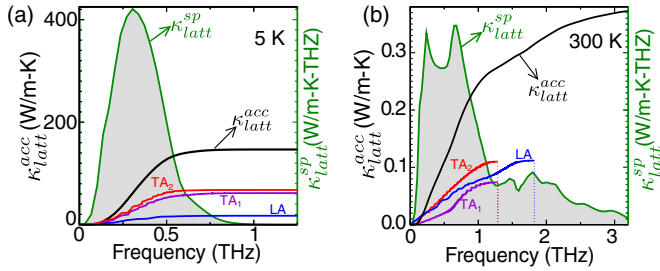
FIG. 4. Accumulative ($\kappa_{\text{latt}}^{\text{acc}}$) and spectral ($\kappa_{\text{latt}}^{sp}$) lattice thermal conductivity as a function of phonon frequency at (a) 5 K and (b) 300 K. The y axes cover the same numerical range in each figure.

Mode-wise contributions to κ_{latt} at low temperature (5 K) and RT are shown in Figs. 4(a) and 4(b), respectively. Here the frequency derivatives of the accumulated thermal conductivity ($\kappa_{\text{latt}}^{\text{acc}}$) were computed, resulting in a spectral thermal conductivity ($\kappa_{\text{latt}}^{sp}$) analogous to a density of states. The spectral thermal conductivity quantifies the contribution of modes in different frequency regions to the overall thermal transport. At low temperatures (5 K) most of the heat is carried by modes in the frequency window 0–0.65 THz [Fig. 4(a)]. The temperature dependence of the branch-wise κ_{latt} is shown in Fig. S3(a) and S3(b) in the SM [28]. At low temperatures both transverse acoustic modes (TA_1 and TA_2) carry nearly similar heat (∼65 W/m-K), whereas contributions of LA phonons are substantially smaller (18 W/m-K). As the temperature increases the higher frequency phonon modes are excited. These contribute both to heat transfer and to scattering, resulting in a general reduction in κ_{latt}. At 300 K [Fig. 4(b)], most heat is carried by phonons in the expanded frequency window 0–2.5 THz. The highest contribution to κ_{latt} stems from the LA phonons (0.11 W/m-K), while TA_1, TA_2, and combined optic contributions are 0.07, 0.10, and 0.08 W/m-K, respectively.

Turning to the impacts of anharmonicity on the κ_{latt} behavior of TlBr, calculated mode Grüneisen parameters are shown in Fig. 3(b). Since the TA_1 phonon frequencies at the M point are most sensitive to lattice expansion, they exhibit the largest Grüneisen parameters shown by the green shaded area. In particular, we observe a Grüneisen parameter ∼9.2 for TA_1 phonons at the M point and ∼7.5 for the soft, nearly ferroelectric Γ-point TO phonons. The TO mode Grüneisen parameters are nearly three times smaller than those in PbTe (∼20 near the zone center) [48], yet TlBr exhibits a much lower κ_{latt}. The strong anharmonicity suggested by the large Grüneisen parameter values in TlBr, in principle, should correspond to strong scattering of the low-frequency heat-carrying phonons. The phonon-phonon scattering rates for the low frequency heat carriers at different lattice strains are shown in Fig. 5(a). The majority (∼90%) of heat in TlBr is carried by phonons with frequencies between 0 and 2.5 THz; thus, only scattering rates within this frequency range are discussed here. The contributions of specific three phonon scattering processes, namely AAA, AAO, and AOO, are shown in Fig. 5(b), where A and O denote acoustic and optic phonons, respectively. To highlight the relative enhancement of scattering rates under strain, these are scaled with respect to total scattering rates in 0–2 THz frequency window at zero strain (SR_0). We find
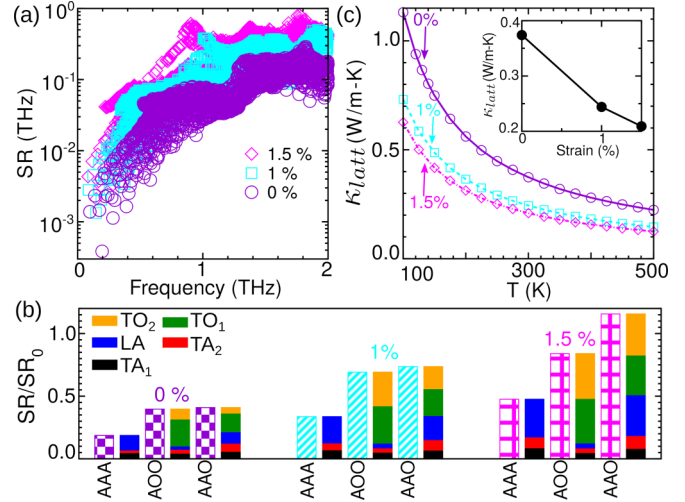

FIG. 5. (a) Room temperature anharmonic scattering rates (SR) as a function of frequency at 0%, 1%, and 1.5% lattice expansion. (b) Contribution of specific three-phonon scattering processes calculated within the 0–2 THz frequency window. Individual contribution from acoustic (TA_1, TA_2, LA), and optic (TO_1, TO_2) phonons, to the three-phonon scattering processes are also shown. These correspond to scattering processes that involve at least one phonon of the indicated polarization. The contribution of individual phonon branches is proportional to the bar height. The scattering rates are scaled with respect to total scattering rate (SR_0) in 0–2 THz frequency range at 0% lattice expansion. (c) Calculated κ_{latt} of TlBr as a function of temperature at 0%, 1%, and 1.5% lattice expansion. The inset shows the behavior of 300 K lattice thermal conductivity under lattice expansion.

that at 0% strain AAO (40%) and AOO (41%) type scattering channels (coalescence and decay processes) dominate the phonon-phonon resistance in TlBr, whereas AAA scattering contributes ∼19%.

Apart from the TA and TO instabilities, another interesting feature mentioned above is an avoided crossing between LA and TO branches at different points in the Brillouin zone. As discussed in previous studies [49–52] this feature can enhance the scattering between these branches and reduce their transport efficiency. We find that nearly 45% of AAO processes involve the LA-LA-TO scattering channel, and 35% of AOO scattering involves the LA-TO-TO scattering channel. This observation agrees with the theory that avoided crossings can induce strong anharmonicity [49–52]. Thus, combined (i) low phonon group velocities, (ii) low-frequency dispersive optical phonons, and (iii) avoided crossings between LA and TO branches give ultralow κ_{latt} in TlBr, the last two inducing significant phonon-phonon scattering.

Next, we examine the proximity of TlBr to a ferroelectric instability with relation to its κ_{latt}. As shown previously, the ferroelectric state in TlBr can be achieved by expanding the lattice parameter by 2% [17]. We calculated κ_{latt} under 1% and 1.5% uniform lattice expansion. The resulting phonon dispersion and RT κ_{latt} are shown in Figs. 3(a) and 5(c), respectively. RT κ_{latt} is significantly reduced with strain ∼44%, going from 0.375 W/m-K (unstrained) to 0.21 W/m-K (1.5%). With lattice expansion the frequencies of all phonons decrease; however, there are two main modifications in the

TABLE I. Calculated TlBr κ_{latt} at 100 and 300 K using 0 K IFCs (0 K harmonic and anharmonic IFCs calculated at the 0 K lattice parameter), quasiharmonic approximation (QHA), and temperature-dependent force constants (TDEP). Within the QHA the temperature dependence is included through the volume. In TDEP calculations the temperature dependence is included in both volume and IFCs. Measured lattice thermal conductivities (κ_{Meas}) are also shown for comparison. The experimental lattice parameter* is measured at 293 K [61]. All first principles calculations are done within PBEsol.

Temperature	0 K IFCs		QHA		TDEP		EXP	
(K)	a (Å)	κ_{Calc} (W/m-K)	a (Å)	$\kappa_{\text{Calc}}^{\text{QHA}}$ (W/m-K)	a (Å)	$\kappa_{\text{Calc}}^{\text{TDEP}}$(W/m-K)	a (Å)	κ_{Meas} (W/m-K)
100	3.8981	1.2	3.91	0.920	3.94	0.99458		1.10
300	3.8981	0.374	3.96	0.184	3.99	0.3508	3.985*	0.49

dispersion: (i) The TO mode frequency at the zone center decreases, and this branch becomes less dispersive along $\Gamma - X$. This brings TlBr much closer to the ferroelectric instability. (ii) The TA_1 mode frequency at the M point sharply decreases. These modifications, along with the overall decrease in phonon frequencies, increase the phonon-phonon scattering under lattice expansion [shown in Fig. 5(a)]. Analysis of individual scattering types (AAA, AOO, and AAO) under lattice expansion within the 0–2 THz window is shown in Fig. 5(b). These contributions represent relative enhancements in scattering processes and are scaled with respect to scattering rates in TlBr with no strain. Under lattice expansion, AAO- and AOO-type scatterings are enhanced by nearly 50%. Phonon polarization analysis shows that these enhancements are mainly driven by TO_1 and TO_2 phonons (modest contributions from LA phonons are also found) as shown in Fig. 5(b). Thus, TO phonons play an important role in inducing strong anharmonic scattering; however, the question remains as to whether these TO phonons mainly belong to the ferroelectric instability or not. To investigate this, we analyze where the TO phonons originate within the Brillouin zone for AOO/AAO-type scattering. We observe that the ferroelectrically active TO phonons near the zone center contribute roughly 18% to the scattering processes, while the remaining contribution comes from all other regions of the Brillouin zone. This suggests that although soft ferroelectric modes are relevant for ultralow κ_{latt}, scattering contributions from phonons in the entire Brillouin zone are equally important. Similar observations were recently made for PbTe [53].

Previous experimental reports [54–56] suggested that thermal expansion in TlBr from low temperature to 300 K is around 1.2%, indicating that lattice parameters of TlBr are sensitive to temperature. Here we include this by two methods: (i) within the quasiharmonic approximation (QHA), where the temperature dependence is included through the volume by following the method described in Refs. [57,58], and (ii) within the TDEP method, where lattice parameters at 100 and 300 K are obtained by minimizing the free energy using *ab initio* molecular dynamics simulations [59] (shown in Fig. S4 of the SM [28]). Additionally, in the TDEP approach the temperature dependence is included in both harmonic and anharmonic IFCs. Phonon dispersions calculated within QHA and TDEP methods are compared in Figs. S5(a) and S5(b) of the SM [28]. Within the QHA the optical modes soften and the zone center TO mode exhibits a strong decrease with increasing temperature as presented in Fig. S5(c) [28]. As found for PbTe [60], when the system is strongly anharmonic the QHA does not predict the correct temperature dependence

of the TO mode. The temperature dependence of the TO mode frequency calculated within TDEP is also shown in Fig. S5(c) [28], where a much weaker temperature dependence is observed. These differences have consequences in the calculation of κ_{latt}.

Table I presents a comparison of κ_{latt} of TlBr calculated using 0-K IFCs (using 0-K lattice parameters and 0-K IFCs), using the QHA, and using the TDEP method at 100 and 300 K. The calculated lattice constants within the QHA are $a_{100\text{K}}^{\text{QHA}} = 3.91$ Å and $a_{300\text{K}}^{\text{QHA}} = 3.96$ Å. Generally, with increasing lattice parameters the κ_{latt} decreases due to phonon softening (generally increased scattering and reduced velocities). Including the effects of lattice expansion within the QHA worsens the agreement between calculated ($\kappa_{\text{Calc}}^{\text{QHA}} = 0.184$ W/m-K) and measured room temperature lattice thermal conductivities ($= 0.49$ W/m-K) at room temperature. The behavior of κ_{latt} calculated within the QHA is related to strong optical phonon softening, which results in enhanced scattering and therefore low κ_{latt}. On the other hand, the TDEP method does a better job in predicting not only the lattice parameter, ($a_{300\text{K}}^{\text{TDEP}} = 3.99$ Å, $a_{300\text{K}}^{\text{EXP}} = 3.985$ Å) but also gives higher 300 K κ_{latt} ($\kappa_{\text{Calc}}^{\text{TDEP}} = 0.35$ W/m-K) in comparison with the QHA. Although TDEP improves the κ_{latt} when compared to QHA, it still underestimates the measured κ_{Meas} by 0.14 W/m-K.

To address the effect of temperature and anharmonicity in the phonon dispersion we also calculated the spectral functions $S(q, E)$ [62,63] at 100 and 300 K as shown in Figs. 6(a) and 6(b), respectively. Details of these calculations can be found in Refs. [41,64]. With increasing temperature, the calculated spectral function exhibits signatures of strongly anharmonic behavior: the energy of the TO modes along
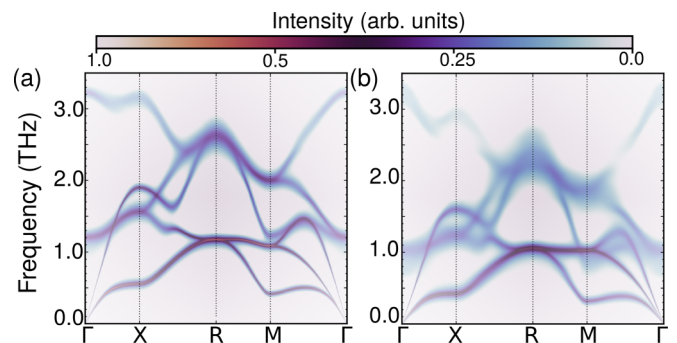

FIG. 6. TlBr spectral function $[S(q, E)]$ calculated at (a) 100 K and (b) 300 K using a q grid of $21 \times 21 \times 21$. The intensities are presented in log scale and normalized to unity.

$\Gamma - M$ and $\Gamma - X$ directions are significantly softened, as discussed above. Furthermore, the phonon bands, optic modes in particular, become more diffuse with increasing temperature suggesting strongly increasing linewidths with increasing temperature. These features are similar to those previously reported for strong anharmonic materials such as PbTe, SnTe, and PbSe [41,64].

IV. SUMMARY

Through a combination of measurements and first principles simulations, we demonstrated that phonons in TlBr are strongly anharmonic, and that this is associated with lattice instabilities. The ultralow κ_{latt} (0.5 W/m-K) found at room temperature stems from surprisingly strong phonon-phonon scattering resistance in this simple binary compound and low phonon group velocities. Polarization analysis of the scattering rates revealed that the scattering resistance is not isolated to ferroelectric soft modes, but rather derives from TO mode scattering throughout the Brillouin zone. Furthermore, we show that the QHA cannot correctly describe the effect of thermal expansion on phonon dispersions and lattice thermal conductivity of TlBr and considering temperature dependence of the IFCs is necessary. Insights into the thermal conductivity behavior of TlBr can be extended to similar compounds where strong anharmonicities have been reported.

[1] J. Garg, N. Bonini, B. Kozinsky, and N. Marzari, Role of Disorder and Anharmonicity in the Thermal Conductivity of Silicon-Germanium Alloys: A First-Principles Study, Phys. Rev. Lett. **106**, 045901 (2011).

[2] W. Kim, J. Zide, A. Gossard, D. Klenov, S. Stemmer, A. Shakouri, and A. Majumdar, Thermal Conductivity Reduction and Thermoelectric Figure of Merit Increase by Embedding Nanoparticles in Crystalline Semiconductors, Phys. Rev. Lett. **96**, 045901 (2006).

[3] B. Poudel, Q. Hao, Y. Ma, Y. Lan, A. Minnich, B. Yu, X. Yan, D. Wang, A. Muto, D. Vashaee, X. Chen, J. Liu, M. S. Dresselhaus, G. Chen, and Z. Ren, High-thermoelectric performance of nanostructured bismuth antimony telluride bulk alloys, Science **320**, 634 (2008).

[4] S. K. Bux, R. G. Blair, P. K. Gogna, H. Lee, G. Chen, M. S. Dresselhaus, R. B. Kaner, and J. Pierre Fleurial, Nanostructured bulk silicon as an effective thermoelectric material, Adv. Funct. Mater. **19**, 2445 (2009).

[5] P. F. P. Poudeu, J. D'Angelo, H. Kong, A. Downey, J. L. Short, R. Pcionek, T. P. Hogan, C. Uher, and M. G. Kanatzidis, Nanostructures versus solid solutions: Low lattice thermal conductivity and enhanced thermoelectric figure of merit in Pb$_{9.6}$Sb$_{0.2}$Te$_{10-x}$Se$_x$ bulk materials, J. Am. Chem. Soc. **128**, 14347 (2006).

[6] G. A. Slack, *Solid State Physics* (Elsevier, Amsterdam, 1979), Vol 34, pp. 1–71.

[7] D. G. Cahill, S. K. Watson, and R. O. Pohl, Lower limit to the thermal conductivity of disordered crystals, Phys. Rev. B **46**, 6131 (1992).

[8] M. T. Agne, R. Hanus, and G. J. Snyder, Minimum thermal conductivity in the context of diffuson-mediated thermal transport, Energy Environ. Sci. **11**, 609 (2018).

[9] S. Mukhopadhyay, D. S. Parker, B. C. Sales, A. A. Puretzky, M. A. McGuire, and L. Lindsay, Two-channel model for ultralow thermal conductivity of crystalline Tl$_3$VSe$_4$, Science **360**, 1455 (2018).

[10] A. Einstein, Elementare betrachtungen über die thermische molekularbewegung in festen körpern, Ann. Phys. **340**, 679 (1911).

[11] M. Simoncelli, N. Marzari, and F. Mauri, Unified theory of thermal transport in crystals and glasses, Nat. Phys. **15**, 809 (2019).

[12] L. Isaeva, G. Barbalinardo, D. Donadio, and S. Baroni, Modeling heat transport in crystals and glasses from a unified lattice-dynamical approach, Nat. Commun. **10**, 3853 (2019).

[13] P. B. Allen and J. L. Feldman, Thermal conductivity of disordered harmonic solids, Phys. Rev. B **48**, 12581 (1993).

[14] A. V. Churilov, G. Ciampi, H. Kim, W. M. Higgins, L. J. Cirignano, F. Olschner, V. Biteman, M. Minchello, and K. S. Shah, TlBr and TlBr$_x$I$_{1-x}$ crystals for γ-ray detectors, J. Cryst. Growth **312**, 1221 (2010).

[15] I. Rahman and R. Hofstadter, Thallium halide radiation detectors, Phys. Rev. B **29**, 3500 (1984).

[16] A. V. Churilov, G. Ciampi, H. Kim, L. J. Cirignano, W. M. Higgins, F. Olschner, and K. S. Shah, Thallium bromide nuclear radiation detector development, IEEE Trans. Nucl. Sci. **56**, 1875 (2009).

[17] H. Kim, L. Cirignano, A. Churilov, G. Ciampi, W. Higgins, F. Olschner, and K. S. Shah, Developing larger TlBr detectors—detector performance, IEEE Trans. Nucl. Sci. **56**, 819 (2009).

[18] I. Oliveira, J. Chubaci, M. Armelin, and M. Hamada, Purification and crystal growth of TlBr for application as a radiation detector, Cryst. Res. Technol. **39**, 849 (2004).

[19] A. Togo, L. Chaput, and I. Tanaka, Distributions of phonon lifetimes in Brillouin zones, Phys. Rev. B **91**, 094306 (2015).

[20] A. Togo and I. Tanaka, First principles phonon calculations in materials science, Scr. Mater. **108**, 1 (2015).

[21] L. Chaput, A. Togo, I. Tanaka, and G. Hug, Phonon-phonon interactions in transition metals, Phys. Rev. B **84**, 094302 (2011).

[22] J. P. Perdew, A. Ruzsinszky, G. I. Csonka, O. A. Vydrov, G. E. Scuseria, L. A. Constantin, X. Zhou, and K. Burke, Restoring the Density-Gradient Expansion for Exchange in Solids and Surfaces, Phys. Rev. Lett. **100**, 136406 (2008).

[23] P. E. Blöchl, Projector augmented-wave method, Phys. Rev. B **50**, 17953 (1994).

[24] G. Kresse and J. Furthmüller, Efficiency of *ab initio* total energy calculations for metals and semiconductors

using a plane-wave basis set, Comput. Mater. Sci. **6**, 15 (1996).

[25] G. Kresse and D. Joubert, From ultrasoft pseudopotentials to the projector augmented-wave method, Phys. Rev. B **59**, 1758 (1999).

[26] X. Gonze, J.-C. Charlier, D. Allan, and M. Teter, Interatomic force constants from first principles: The case of α-quartz. Phys. Rev. B **50**, 13035 (1994).

[27] X. Gonze and C. Lee, Dynamical matrices, Born effective charges, dielectric permittivity tensors, and interatomic force constants from density-functional perturbation theory, Phys. Rev. B **55**, 10355 (1997).

[28] See Supplemental Material at http://link.aps.org/supplemental/10.1103/PhysRevMaterials.4.045403 for additional details on the experimental measurements, computational methods, scattering rates, and temperature dependent effective potential method.

[29] W. Lawless, Specific heat and thermal-conductivity measurements on cesium and thallous halide crystals at low temperatures, Phys. Rev. B **30**, 6057 (1984).

[30] O. Hellman, P. Steneteg, I. A. Abrikosov, and S. I. Simak, Temperature dependent effective potential method for accurate free energy calculations of solids, Phys. Rev. B **87**, 104111 (2013).

[31] S.-i Tamura, Isotope scattering of large-wave-vector phonons in GaAs and InSb: Deformation-dipole and overlap-shell models, Phys. Rev. B **30**, 849 (1984).

[32] A. Ioffe and A. Regel, *Non-crystalline, Amorphous and Liquid Electronic Semiconductors*, Vol. 4 (Wiley, New York, 1960).

[33] N. K. Ravichandran and D. Broido, Unified first-principles theory of thermal properties of insulators, Phys. Rev. B **98**, 085205 (2018).

[34] Y. Xia and M. K. Chan, Anharmonic stabilization and lattice heat transport in rocksalt β-GeTe, Appl. Phys. Lett. **113**, 193902 (2018).

[35] Y. Xia, Revisiting lattice thermal transport in PbTe: The crucial role of quartic anharmonicity, Appl. Phys. Lett. **113**, 073901 (2018).

[36] Y. Xia, K. Pal, J. He, V. Ozoliņš, and C. Wolverton, Particlelike Phonon Propagation Dominates Ultralow Lattice Thermal Conductivity in Crystalline Tl_3VSe_4, Phys. Rev. Lett. **124**, 065901 (2020).

[37] O. Hellman, I. A. Abrikosov, and S. I. Simak, Lattice dynamics of anharmonic solids from first principles, Phys. Rev. B **84**, 180301 (2011).

[38] O. Hellman and I. A. Abrikosov, Temperature-dependent effective third-order interatomic force constants from first principles, Phys. Rev. B **88**, 144301 (2013).

[39] E. Cowley and A. Okazaki, The lattice dynamics of thallous bromide, Proc. Roy. Soc. London Ser. A **300**, 45 (1967).

[40] M.-H. Du and D. J. Singh, Enhanced Born charge and proximity to ferroelectricity in thallium halides, Phys. Rev. B **81**, 144114 (2010).

[41] C. W. Li, O. Hellman, J. Ma, A. F. May, H. B. Cao, X. Chen, A. D. Christianson, G. Ehlers, D. J. Singh, B. C. Sales, and O. Delaire, Phonon Self-Energy and Origin of Anomalous Neutron Scattering Spectra in SnTe and PbTe Thermoelectrics, Phys. Rev. Lett. **112**, 175501 (2014).

[42] J. An, A. Subedi, and D. J. Singh, *Ab initio* phonon dispersions for PbTe, Solid State Commun. **148**, 417 (2008).

[43] O. Delaire, J. Ma, K. Marty, A. F. May, M. A. McGuire, M. H. Du, D. J. Singh, A. Podlesnyak, G. Ehlers, M. D. Lumsden, and B. C. Sales, Giant anharmonic phonon scattering in PbTe, Nat. Mater. **10**, 614 (2011).

[44] A. Banik, T. Ghosh, R. Arora, M. Dutta, J. Pandey, S. Acharya, A. Soni, U. V. Waghmare, and K. Biswas, Engineering ferroelectric instability to achieve ultralow thermal conductivity and high thermoelectric performance in $Sn_{1-x}Ge_xTe$, Energy Environ. Sci. **12**, 589 (2019).

[45] C. W. Li, J. Hong, A. F. May, D. Bansal, S. Chi, T. Hong, G. Ehlers, and O. Delaire, Orbitally driven giant phonon anharmonicity in SnSe, Nat. Phys. **11**, 1063 (2015).

[46] L. D. Zhao, S. H. Lo, Y. Zhang, H. Sun, G. Tan, C. Uher, C. Wolverton, V. P. Dravid, and M. G. Kanatzidis, Ultralow thermal conductivity and high thermoelectric figure of merit in SnSe crystals, Nature (London) **508**, 373 (2014).

[47] Y. Zhang, X. Ke, P. R. Kent, J. Yang, and C. Chen, Anomalous Lattice Dynamics Near the Ferroelectric Instability in PbTe, Phys. Rev. Lett. **107**, 175503 (2011).

[48] S. Lee, K. Esfarjani, T. Luo, J. Zhou, Z. Tian, and G. Chen, Resonant bonding leads to low lattice thermal conductivity, Nat. Commun. **5**, 3525 (2014).

[49] M. Christensen, A. B. Abrahamsen, N. B. Christensen, F. Juranyi, N. H. Andersen, K. Lefmann, J. Andreasson, C. R. H. Bahl, and B. B. Iversen, Avoided crossing of rattler modes in thermoelectric materials, Nat. Mater. **7**, 811 (2008).

[50] W. Li, J. Carrete, G. K. Madsen, and N. Mingo, Influence of the optical-acoustic phonon hybridization on phonon scattering and thermal conductivity, Phys. Rev. B **93**, 205203 (2016).

[51] W. Li and N. Mingo, Ultralow lattice thermal conductivity of the fully filled skutterudite $YbFe_4Sb_{12}$ due to the flat avoided-crossing filler modes, Phys. Rev. B **91**, 144304 (2015).

[52] T. Pandey, C. A. Polanco, L. Lindsay, and D. S. Parker, Lattice thermal transport in $La_3Cu_3X_4$ compounds ($X = P$, As, Sb, Bi): Interplay of anharmonicity and scattering phase space, Phys. Rev. B **95**, 224306 (2017).

[53] S. Ju, T. Shiga, L. Feng, and J. Shiomi, Revisiting PbTe to identify how thermal conductivity is really limited, Phys. Rev. B **97**, 184305 (2018).

[54] R. Srinivasan, G. Lakshmi, and V. Ramachandran, Mode Gruneisen parameters and thermal expansion of thallous bromide, J. Phys. C **8**, 2897 (1975).

[55] A. D. Redmond and B. Yates, The low temperature thermal expansion of thallous chloride and thallous bromide, J. Phys. C **5**, 1589 (1972).

[56] R. A. Secco, Q. Chen, E. A. Secco, J. Chen, M. T. Vaughan, J. Z. Zhang, and G. Chen, Bulk modulus and high pressure thermal expansion of TlCl and TlBr, Solid State Commun. **107**, 553 (1998).

[57] P. B. Allen, Zero-point and isotope shifts: relation to thermal shifts, Philos. Mag. B **70**, 527 (1994).

[58] L. Lindsay, Isotope scattering and phonon thermal conductivity in light atom compounds: LiH and LiF, Phys. Rev. B **94**, 174304 (2016).

[59] S. Nosé, A molecular dynamics method for simulations in the canonical ensemble, Mol. Phys. **52**, 255 (1984).

[60] A. Romero, E. Gross, M. Verstraete, and O. Hellman, Thermal conductivity in PbTe from first principles, Phys. Rev. B **91**, 214310 (2015).

[61] A. Smakula and J. Kalnajs, Precision determination of lattice constants with a Geiger-counter x-ray diffractometer, Phys. Rev. **99**, 1737 (1955).

[62] R. Cowley, Anharmonic crystals, Rep. Prog. Phys. **31**, 123 (1968).

[63] A. Maradudin and A. Fein, Scattering of neutrons by an anharmonic crystal, Phys. Rev. **128**, 2589 (1962).

[64] N. Shulumba, O. Hellman, and A. J. Minnich, Intrinsic localized mode and low thermal conductivity of PbSe, Phys. Rev. B **95**, 014302 (2017).